382 | https://doi.org/10.3311/PPch.37018
Creative Commons Attribution

Periodica Polytechnica Chemical Engineering, 68(3), pp. 382–397, 2024

Microstructure and Corrosion Study on Friction Surfaced Aluminum Alloy Coatings over Mild Steel

Vinodh Sivalingam[1*], Ramakrishnan Thirumalaisamy[1]

[1] Department of Mechanical Engineering, Sri Eshwar College of Engineering, Kondampatti, Vadasithur Road, 641202 Coimbatore, Tamil Nadu, India
[*] Corresponding author, e-mail: vinodh.s2023ftscholar@sece.ac.in

Received: 31 March 2024, Accepted: 17 July 2024, Published online: 12 August 2024

Abstract

In this study, the low-carbon steel (AISI 1018 mild steel) substrate is coated with the aluminum alloys AA6082-T6, Al-20Zn, and Al-2Si-15SiC to improve its corrosion resistance by the friction surfacing (FS) technique. To produce a high-quality coating, friction surfacing process variables including spin speed, speed of travel, and the rate of feed are crucial. This experiment examines twelve friction-surfaced plates with different parameter combinations. Scanning electron microscopy (SEM) and energy dispersive X-ray spectroscopy (EDS) examinations were carried out in order to comprehend the microstructure and chemical composition of the coating deposits and the area in contact between the coated surface and the substrate. Microstructure investigation reveals that the intermetallic combination of Fe-Al at the coating interface region is an effect of the elemental diffusion of Fe to aluminum at the contact interface. Then a uniform and fine-grained coating deposit is observed as a result of the continuous recrystallization of the consumable rod under frictional stress and heat generation. According to the outcomes of the microhardness test, the coated surface is roughly 15–16% harder than the consumable rod. The coating bond strength was measured using a ram tensile test, and it ranged from 102 MPa to 135 MPa. Finally, evaluation of corrosion behavior through immersion testing and pitting corrosion testing reveals that the coatings made of Al-20Zn and Al-2Si-15SiC exhibit good corrosive resistance in an alkaline environment.

Keywords

friction surfacing, mild steel, AA6082-T6, Al-Zn alloy, Al-Si-SiC composite, corrosion test

1 Introduction

Mild steel has many applications due to its excellent mechanical characteristics and comparatively low cost, but it has poor corrosion resistance, limiting its application in the marine environment [1, 2]. In marine environments, high chloride levels, dissolved oxygen, variable temperatures, the UV rays of the sun, and microbial species are some of the reasons contributing to high corrosion rates for low-carbon steels [3]. To overcome these difficulties, various corrosive resistance coatings are applied to mild steel for its application in the marine environment. Aluminum and its alloy have high corrosive resistance and are used as anti-corrosion coatings for low-carbon steels [4]. The aluminum 6082-T6 alloy has good formability and mechanical properties; it also has excellent corrosion resistance, making it suitable for a wide range of applications in the marine environment [5, 6]. Aluminum-based metal matrix composites typically use silicon carbide as reinforcement to enhance corrosion and wear resistance. Aluminum reinforcement with 15% SiC particles results in an increase in tensile strength, hardness, and wear resistance [7, 8]. Al-SiC composites outperformed pure aluminum in terms of corrosion resistance in an aqueous solution that contains 3.5 weight % sodium chloride. The corosion resistance of the Al/SiC composites increased as the volume fraction of SiC particles increased [9, 10]. It is better than pure aluminum that Al-Si alloys are strengthened with SiC because they are less dense, have better mechanical properties, conduct heat well, and do not rust [11–13]. Al alloying with other elements, such as silicon and magnesium, to create a coating on steel will prevent reactions with chloride ions in seawater and provide a shielding effect for the corrosion environment [14]. Steel is well protected after lengthy immersion in the solution of saline owing to the 19 weight% of Zn in Al, which also helps steel retain its sacrificial nature. Major influences on corrosion behavior are caused by the amount of zinc available in aluminum.

Cite this article as: Sivalingam, V., Thirumalaisamy, R. "Microstructure and Corrosion Study on Friction Surfaced Aluminum Alloy Coatings over Mild Steel", Periodica Polytechnica Chemical Engineering, 68(3), pp. 382–397, 2024. https://doi.org/10.3311/PPch.37018

These alloys have some extremely intriguing features that protect steel [15, 16]. A large number of voids in the Al-Zn coating on steel produced by the arc spray technique have led to decreased corrosion resistance; the corrosion media penetrates into the coating pore and causes internal corrosion on the steel surface [17, 18].

Usually, hot dip and thermal spray techniques are fusion coating techniques that are the most commonly used coating techniques for depositing aluminum and its alloy on steel. In fusion coating, defects such as porosity, blowholes, and surface cracks are unavoidable [19, 20]. To overcome these difficulties, the friction surfacing (FS) coating technique is preferred. Fig. 1 illustrates the FS process, a solid-state coating technique that unites two materials by applying high pressure and frictional heat [21, 22]. The FS coating technique is employed for the repair of damaged or worn components, hard facing, increasing corrosion resistance, improving the surface qualities of parts and tools at a specific location, and creating metal matrix composites [23–25]. The potential to deposit materials that are metallurgically incompatible with metals, little dilution, and a small heat-affected zone are the most notable advantages of FS over other coating processes. In contrast to fusion-based methods, connecting materials that are not the same has an advantage because the highest temperature stays below the melting point of the rod due to friction, which reduces the number of holes and cracks that form when the materials solidify [26–28]. The aluminum alloy A356 surface is friction-surfaced with a SiC reinforced AA 2124 composite. The creation of a strong metallurgical bond with the substrate is responsible for the excellent corrosion and wear resistance of the coating [29].

The procedure parameters significantly influence the quality of the frictional surface layer. Faster travel led to thicker deposits, higher deposition hardness, and reduced energy consumption. Wider and thinner deposits were produced when the axial force was increased; however, excessive force led to an uneven deposition [30]. The axial pressure, traverse speed, and rotating speed all worked together to influence the coating thickness. The augmentation in axial load resulted in the formation of a coating without any defects at the interface in the in FS of Al6061 alloy [31].

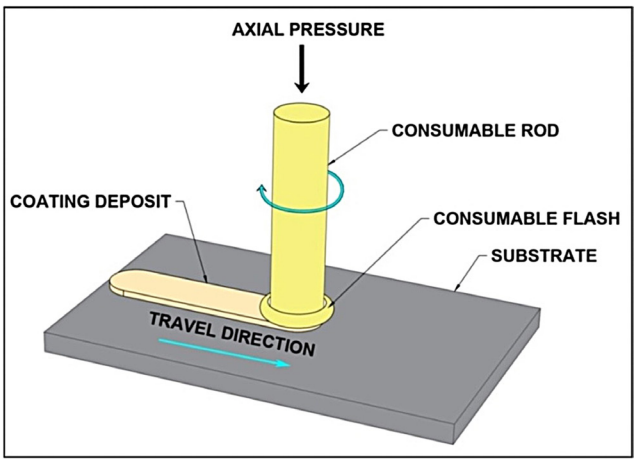

Fig. 1 Friction surfacing process

Despite the fact that low-carbon steel has a lot of applications that call for coatings made of aluminum alloy, some of them include coating for underwater vehicles, turbine blades, crack and damage restoration for marine bodies, shipbuilding, and the construction of oil and gas platforms. As a result, the primary focus of this work is on the newly created friction surfacing of AA6082-T6, Al-19Zn, and Al-2Si-15SiC alloys on mild steel, utilizing them for application in corrosive environments. We subject the coated surface, interface, and substrate to microstructure investigation and elemental mapping. Then, in four distinct pH media, the corrosion responses of the three distinct coated surfaces and the untreated surfaces are examined and reported herein.

2 Materials and procedures for experiments

2.1 Materials

The substrate was made of a 10 mm thick mild steel plate that was cut to measurements of 75 mm by 150 mm. Then the three different consumables as AA6082-T6, Al-19Zn, and Al-2Si-15SiC, are prepared through stir casting. Aluminum (Al1050), which is 99% pure in nature, was used as a matrix material. As reinforcement, 2% silicon and 15% silicon carbide powder with a normal grain size of 40 μm are utilized. Initially, the aluminum is melted to a liquid state in the stir casting furnace, and the reinforcement Si and SiC are preheated at 1000 °C to avoid the moisture content being added to the liquid aluminum. Magnesium is added to the mixture in tiny amounts (0.5–1 weight %) in order to boost the fluidity of the molten metal. Additionally, Mg also strengthens the connection between the reinforcement and the matrix [12]. The mixture is stirred properly for 30 min to ensure a uniform distribution of reinforcement in the aluminum matrix. Next, the liquefied composite material is poured into a cylindrical die, and the cast rod is machined to 20 mm diameter and 100 mm length, which is used as a consumable for FS. Similarly, we use stir casting to produce Al-19Zn. The chemical composition of Al-Si-SiC and Al-Zn is presented in Tables 1 and 2, respectively.

Table 1 Chemical composition of Al-2Si-15SiC

Composition weight %					
SiC	Si	Mg	Fe	Cu	Al
15	2	0.5	0.5	0.1	Balance

Table 2 Chemical composition of Al-19Zn

Composition weight %				
Zn	Mg	Fe	Cu	Al
19	1	0.5	0.1	Balance

Then AA6082-T6, the special grade aluminum alloy used for welding and corrosion environments, is readily available in the form of a plain rod machined for the above-mentioned dimensions, and its chemical composition is presented in Table 3.

2.2 Friction surfacing method and process parameter

A friction stir welding machine with positional and load controllers was used to carry out the friction surfacing procedure. Before the experimental operation, the steel substrate plates were securely connected at the sides in a manner parallel to the motion of the spinning rod. The substrate was milled to create a flat, oxide-free surface, and the end of the consumable rod was machined for absolute flatness. To avoid contamination, the substrate and coated rod were cleaned with acetone before surfacing. The substrate roughness was maintained between 5.9 μm and 7 μm to improve the generation of friction force between the consumable and the substrate surface. A 20 s dwell time was used to maintain consistency throughout coating depositions [22]. The process parameters were chosen using a literature analysis and the number of trials carried out in this study. Fig. 2 illustrates the experimental setup for the FS process.

2.3 Material characterization and microstructure analysis

The SEM analysis is done by ZEISS EVO 50 at 15 to 20 kV for the three different aluminum composition coatings. Samples of 10 mm × 10 mm were polished using emery sheets of grades 1000 and 2000, followed by alumina gel for scratch removal. Mirror finishing was added by utilizing diamond paste for further polishing of the samples. The elements and proportion of elements present at random points in composites were analyzed using EDS coupled with SEM, and line mapping was also performed along the region referred to as the coating, interface, and substrate [20, 21].

Table 3 Chemical composition of AA6082-T6

Composition weight %					
Al	Si	Mg	Fe	Cr	Zn
96	1.3	1.2	0.5	0.25	0.2

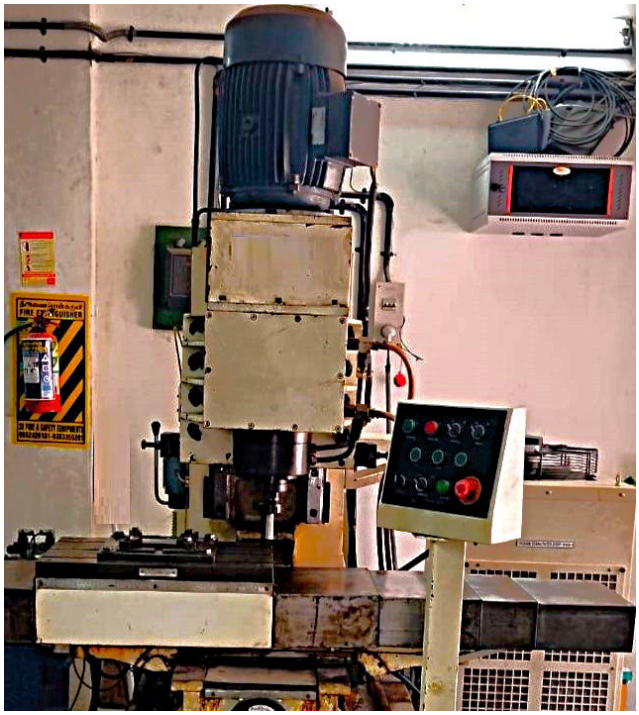

Fig. 2 Friction surfacing process setup

2.4 Bond strength test

Ram tensile testing is employed in the universal testing machine (UTM) to determine how effectively the substrate is adhered to by the coating deposit layer. These methods make it possible to ensure that the sample will break at the interface when subjected to a tensile force, which corresponds to bond strength.

The MIL-J-24445A (SH) standard [32] was specifically used in the design of the ram tensile fixture. The mild steel substrate was sized into the shape of an 8 mm inner hole to create a concentric space between the coating layer and substrate. To effectively clamp the specimen on the laid-out fixture, the surfaces were suitably machined. The annular region, which was only meant for loading, is shown in Fig. 3. The 6 mm diameter push rod is used to apply force to the coating deposit to evaluate the bond strength [25].

2.5 Coating density

The density of the material is used to calculate the corrosion rate. According to ASTM B311-22 [33], the water displacement technique (Archimedean method) was used

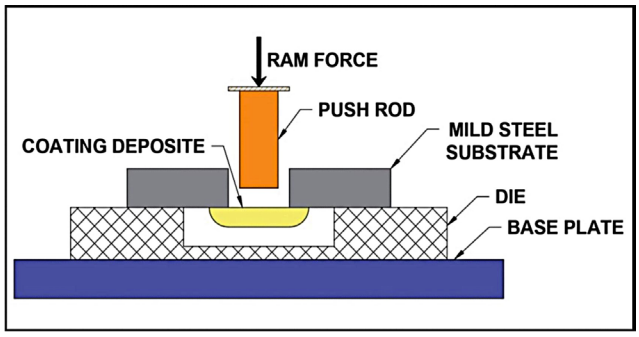

Fig. 3 Bond strength testing method (Ram tensile test)

to determine the density of the coating deposit. Using the law of mixing, the theoretical density of the sample was determined using Eq. (1) [9]:

$$\rho_s = \left[\frac{M_a}{M_a - M_w}\right] \times \rho_w, \quad (1)$$

where ρ_s – actual density of sample, ρ_w – density of water, M_a – sample mass in air and M_w – sample mass in water.

The samples are weighed with an accuracy of 0.1 mg using an electronic balance. The calculated density values are shown in Table 4.

2.6 Micro hardness test

The hardness of the coating deposit and the consumable rod used for coating is measured through the Vickers microhardness test. The indentations were placed on the coating surface at three distinct points in both transverse and longitudinal directions. The same indentation is also made on the three different aluminum composition consumable rods. The standard load of 10 N and a uniform dwell time of 15 s are maintained throughout the test [28].

Table 4 Bond strength and coating density

Sample	Coated material	Bonding strength (MPa)	Average coating density (g/cm³)
S-1	AA6082-T6	102	2.71
S-2		106	
S-3		135	
S-4		132	
S-5	Al-19Zn	109	3.98
S-6		135	
S-7		118	
S-8		109	
S-9	Al-2Si-15Sic	112	2.77
S-10		142	
S-11		139	
S-12		135	

2.7 Chemical resistance test

2.7.1 Immersion corrosion test

The ASTM G31-21 [34] criteria are followed when conducting the immersion corrosion test to gauge the corrosion resistance of the materials. The test samples, with a size of 20 × 20 × 3 mm, are prepared. The test involves immersing the material in different pH solutions, as pH 3, pH 5, pH 7, and pH 9. By combining 200 mL pure water with 2 mL concentrated HCl, a pH of 3 was set. Similar steps were taken to adjust the solution to the required pH by adding HCl for pH 5. Then pH 7 and pH 9 are prepared by adding NaOH and NaCl solutions to the distilled water. The desired pH level is confirmed using a pH meter. After the preparation of four different pH solutions, the coated and uncoated samples are immersed independently for 24, 48, 72, 96, and 120 h in each pH media.

2.7.2 Pitting corrosion test

The three different aluminum composition coatings and substrate material were put through the potential dynamic polarization test, and the samples measuring 1 cm² were exposed to the electrolyte for one hour. Potentiodynamic anodic polarization tests were carried out in accordance with ASTM G5-14(2021) [35] in a solution of 3.5% NaCl at a scan rate of 1 mV/s and over a voltage range of 0.5–0.9 V at a temperature of 25 °C. A saturated calomel electrode served as the reference electrode, and a platinum electrode served as an auxiliary electrode [36, 37].

3 Results and discussion

3.1 Quality of the deposit

The coating deposition quality of FS is greatly influenced by the forging pressure, rotation speed, and feed rate; therefore, 12 samples are friction-surfaced with varied parameter combinations as presented in Fig. 4.

The different parameter combinations and the deposition quality observed through visual inspection are shown in Table 5. For the AA6082-T6 coating, it was found that the bonding was intermittent and uneven overlaying with a constant rotating speed of 900 rpm and a constant pressure of 4 bar in samples S1 and S2. Then, for S3 and S4, continuous and uniform coating is obtained by increasing the forging pressure to 5 bar and speed to 1100 rpm by maintaining a constant feed of 80 mm/min. In the case of Al-19Zn, a uniform and good coating deposit is obtained in sample S6 alone. In the Al-Si-SiC consumable rod, a uniform and continuous coating is observed in samples S10 and S11 for an increased load of 5 bar and at 1200 rpm with a feed rate of 80 mm/min.

Fig. 4 Friction surfaced coating appearance for various parameter combinations listed in Table 5

Table 5 FS coating outcomes for various parameter combination

Sample	Coating rod	Pressure (bar)	Spindle speed (rpm)	Travel speed (mm/min)	Outcomes	Acceptance
S-1	AA6082-T6	4	900	60	Intermittent and uneven deposition	No
S-2		4	1000	80	Discontinuous deposit	No
S-3		5	1100	80	Continuous, good overlaying throughout the bead	Yes
S-4		5	1100	80	Continuous and uniform thickness with narrow deposition	Yes
S-5	Al-19Zn	4	1500	80	Discontinuous and uneven deposition	No
S-6		5	1200	60	Continuous and uniform thickness with narrow deposition	Yes
S-7		5	1200	80	Discontinuous, varying width and poor coating deposit	No
S-8		4	1100	80	Continuous but uneven coating width	No
S-9	Al-2Si-15Sic	5	1400	60	Non uniform, continuous deposit	No
S-10		5	1200	80	Continuous, uniform, narrow deposition and very good overlaying	Yes
S-11		5	1200	80	Continuous but uneven coating width	Yes
S-12		5	900	60	Poor deposition and uneven ripples and bead	No

The same process parameter is adopted for both S10 and S11 samples.

3.2 FE-SEM and EDS analysis

The SEM picture of AA6082-T6, Al-19Zn, and Al-2Si-15SiC coating cross sections is shown in Fig. 5 (b), (d), and (f), respectively, and it reveals a well-bonded interface and no signs of porosity there. Then the SEM image of three different aluminum composition consumable rods is displayed in Fig. 5 (a), (c), and (e). From the test, it is noted that the average grain size of AA6082-T6, Al-19Zn, and Al-2Si-15SiC consumable rods used for FS ranges from 56 µm to 65 µm approximately, while for the three different aluminum composition-coated surfaces of the samples (S3, S6, and S10), it is measured at 5.5 µm to 12 µm, as depicted in Fig. 6. It is found that the overall reduction in the grain size obtained for three different composition-coated surfaces is 70–80% in comparison with the

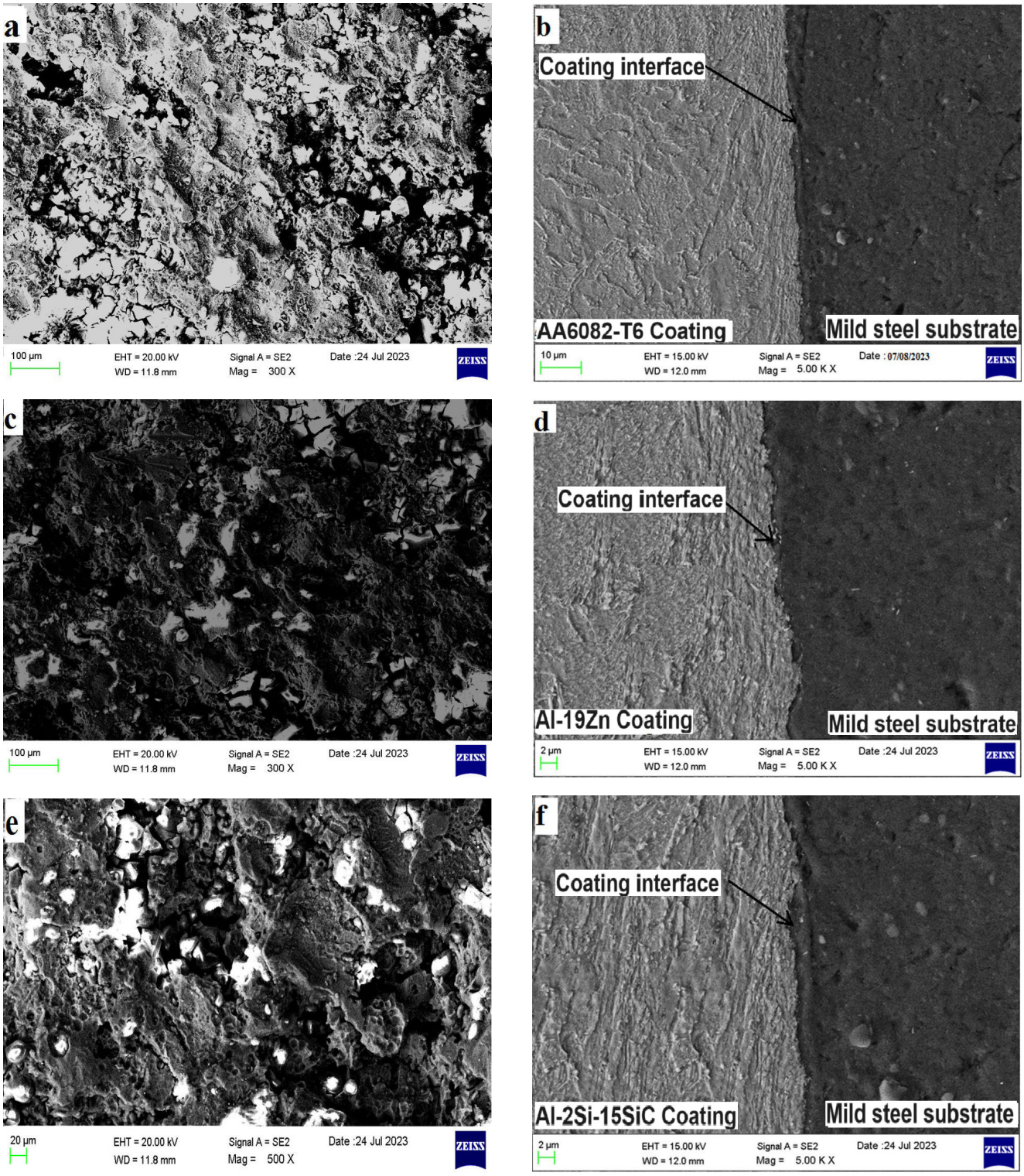

Fig. 5 SEM image of coating, interface and substrate at 500× magnification (a) Al6082-T6 consumable rod, (b) Al6082-T6 coating, (c) Al-19Zn consumable rod, (d) Al-19Zn rod coating, (e) Al-2Si-15Sic consumable rod, (f) Al-2Si-15Sic coating

grain size observed for the consumable rods used in FS. This is because while the tool is moving, the intense plastic flow causes the coarse aluminum grains to break into fine grains, allowing them to distribute equally [26, 27]. The fine and equiaxed morphology of the coating is mostly formed through dynamic recrystallization. An increase in temperature or a drop in plastic strain enlarges the recrystallized grain size, while an increase in plastic strain and a decrease in temperature produce fine grains [38–40].

The consumable rod undergoes thermo-mechanical changes during processing, which results in a reduction in the grain size of the deposited material.

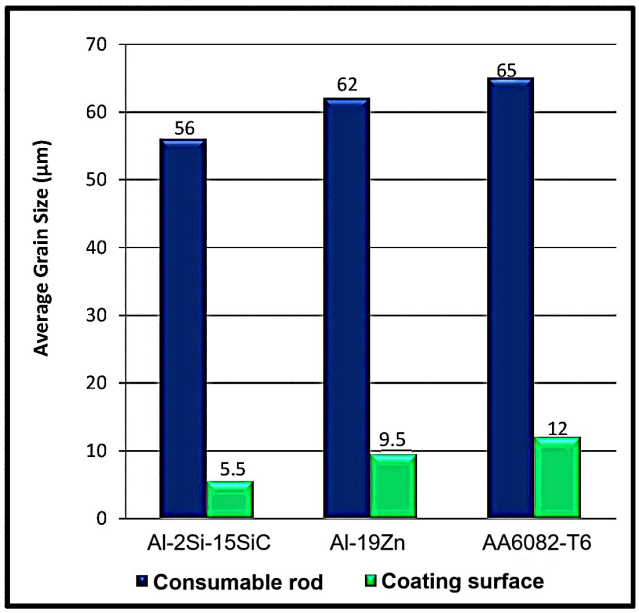

Fig. 6 Average grain size of coating surface and consumable rod

For three different composition-coated samples, the EDS line mapping along the coated surface, interface, and substrate is done. For sample 3 (AA6082-T6), it is evident that the substrate and the covering materials mix at the interface region and form a third-phase FeAl at the interface, as depicted in Fig. 7 (a). Then the Fig. 7 (b) reveals the dispersion of Fe in the coating deposit layer, which forms a strong intermetallic link, whereas Fig. 7 (c) illustrates an uneven dispersion of aluminum particles at the interface with the iron layer. Then, a homogeneous and uniform distribution of Si and Mg on the aluminum composition-coated surface is seen in Fig. 7 (d) and (e). In the case of the Al-19Zn coating (S6), a comparable intermetallic combination of Fe and Al at the interfacial region is seen in Fig. 8 (a). Fig. 8 (b) and (c) shows how Fe and Al are mutually diffusing at the coating interface area. The distribution of Zn on the Al coating deposit surface is presented in Fig. 8 (d). Similarly, for the Al-Si-SiC (S10) coating, it is seen that there is a third phase of Fe-Si and Fe-Al present at the interface, separating the aluminum from the mild steel recorded in Fig. 9 (a). Between aluminum and carbon steel, a thin composite layer formed that resembled the material transfer under the frictional condition. In Fig. 9 (b) and (c), the diffusion of the coating and substrate material is depicted at the interface region. The elemental distribution of Si and C is found to be almost homogeneous on the coating surface, as shown in Fig. 9 (d) and (e), respectively. For all three samples, it confirms that the mild steel and aluminum did mix along the interface, forming a third phase (Fe_3Al). Inevitably, the intermetallic compound formed during FS due to the elemental migration of Fe from the steel to the aluminum alloy caused by the thermo-mechanical effect.

In addition, elemental details for specimens 3, 6, and 10 were examined in the middle region of the deposition interface through the EDS spot analysis shown in Fig. 10, which provides information on the composition of the essential components. In Fig. 10 (a) for the AA6082-T6 coating, spectral data demonstrate the presence of Al, Fe, Si, Mg, C, and O at the interface that forms a metallic composite at the interface region. In Fig. 10 (b) for Al-19Zn, it is found that Al, Fe, Zn, C, and O elements mixed together and formed a strong composite bond at the coating interface. Similarly, in the case of the Al-2Si-15SiC-coated sample of Al, Si, C, Mg, and O found in the Fe interface region, the carbon content at its interface is 9.91%, indicating a stronger bonding between carbon steel and aluminum, as noted in Fig. 10 (c). Then the results also show that all three tested samples had an oxide level at the interface of the coatings. The oxide present in the coating will be advantageous because aluminum oxide or alumina, which is a refractory material, ceramic in nature, and creates hard material, would enhance the hardness of the coating deposit. As the amount of oxide increases, the hardness of the coating will also increase [40]. The elemental mapping at the contact confirms that the material transfer occurs under frictional conditions due to inter-diffusion at the contact interface. During friction surfacing, broken Fe particles are incorporated in a soft Al layer and become deposited. Deposited Al had tiny Fe particles that were scattered throughout it, showing that Al and Fe are mechanically adhered to the area where the coating and substrate meet.

Aluminum, titanium, and chromium oxides are harder than their metals. This hardness enhancement improves coating wear, scratch resistance, and durability. On the flip side, these oxide layers can reduce coating-substrate adhesion energy. When metal interacts with oxide rather than metal, the adhesion energy decreases [41–43]. In this experimental study, the coating surface primarily forms oxide, whereas the interface only exhibits a slight presence of oxide. Simultaneously, at the interface, the substrate-coating materials experience mutual diffusion, resulting in a strong interlocking phenomenon. Because of this diffusion effect, a small amount of oxide at the interface does not have a significant impact on bonding strength.

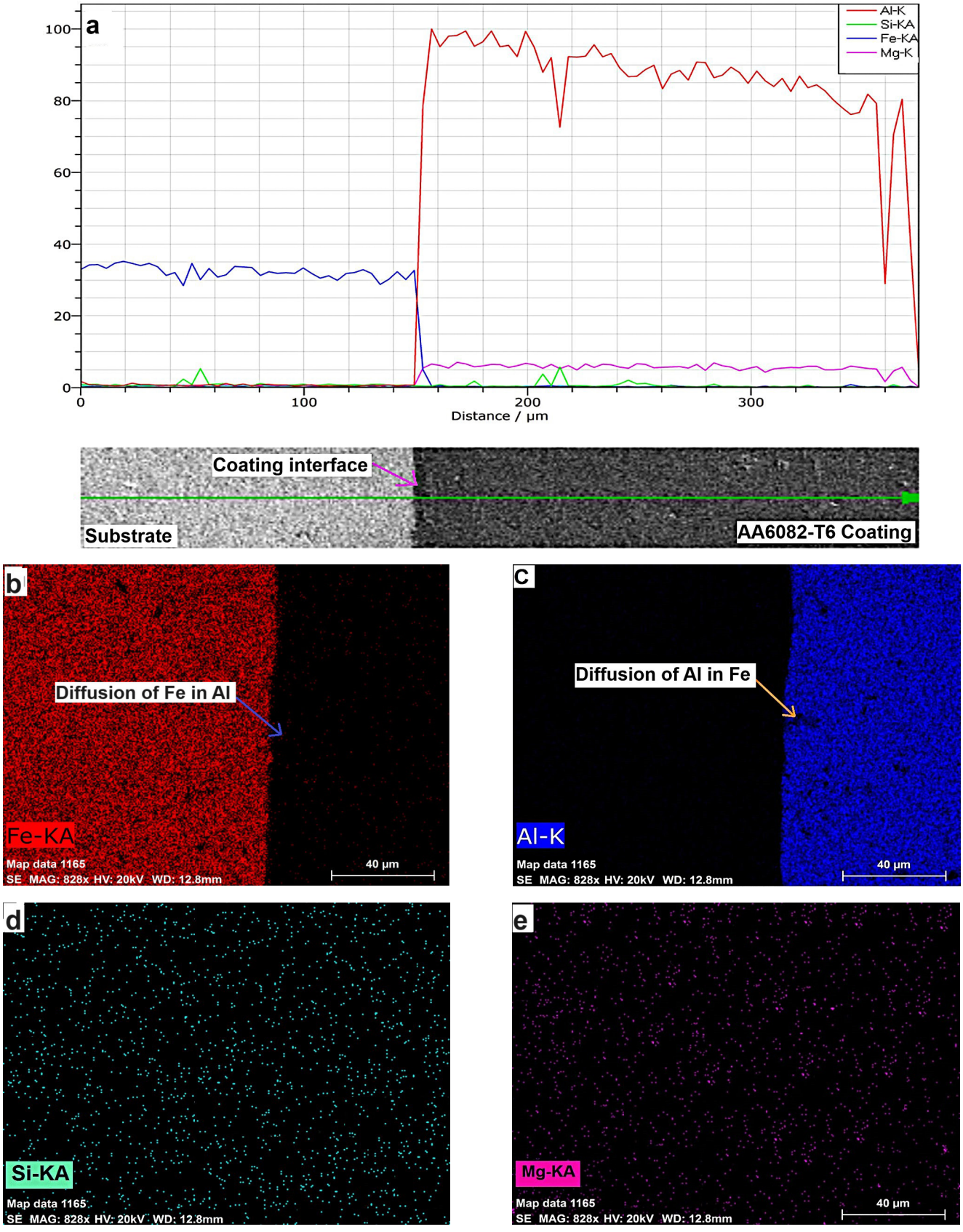

Fig. 7 EDS analysis on AA6082-T6: (a) Graphs of line scanning at interface from coating surface to substrate, (b) Fe distribution at coating and interface region, (c) Al distribution at coating and interface region, (d) Zn distribution on coating surface

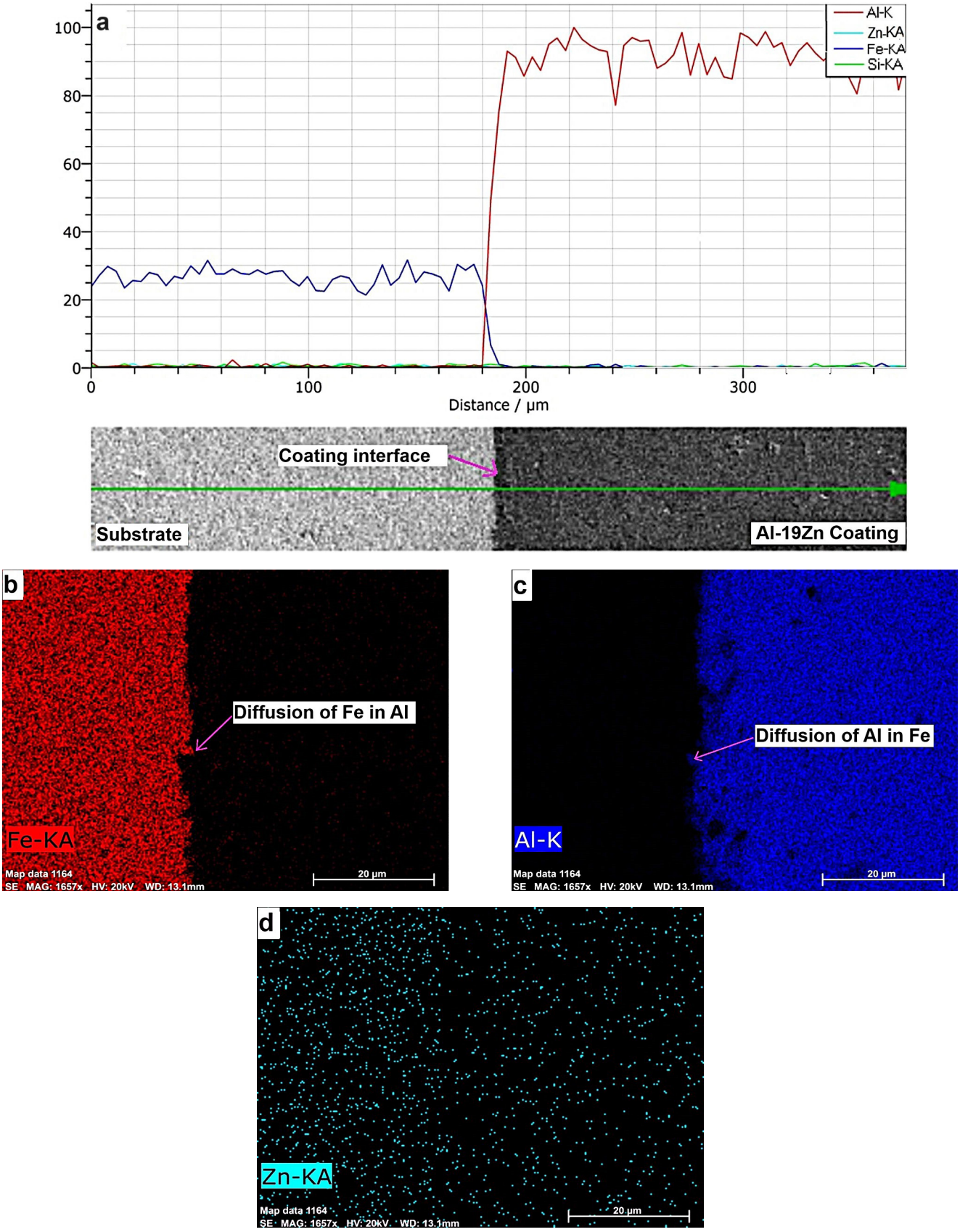

Fig. 8 EDS analysis on Al-19Zn: (a) Graphs of line scanning at interface from coating surface to substrate, (b) Fe distribution at coating and interface region, (c) Al distribution at coating and interface region, (d) Zn distribution on coating surface

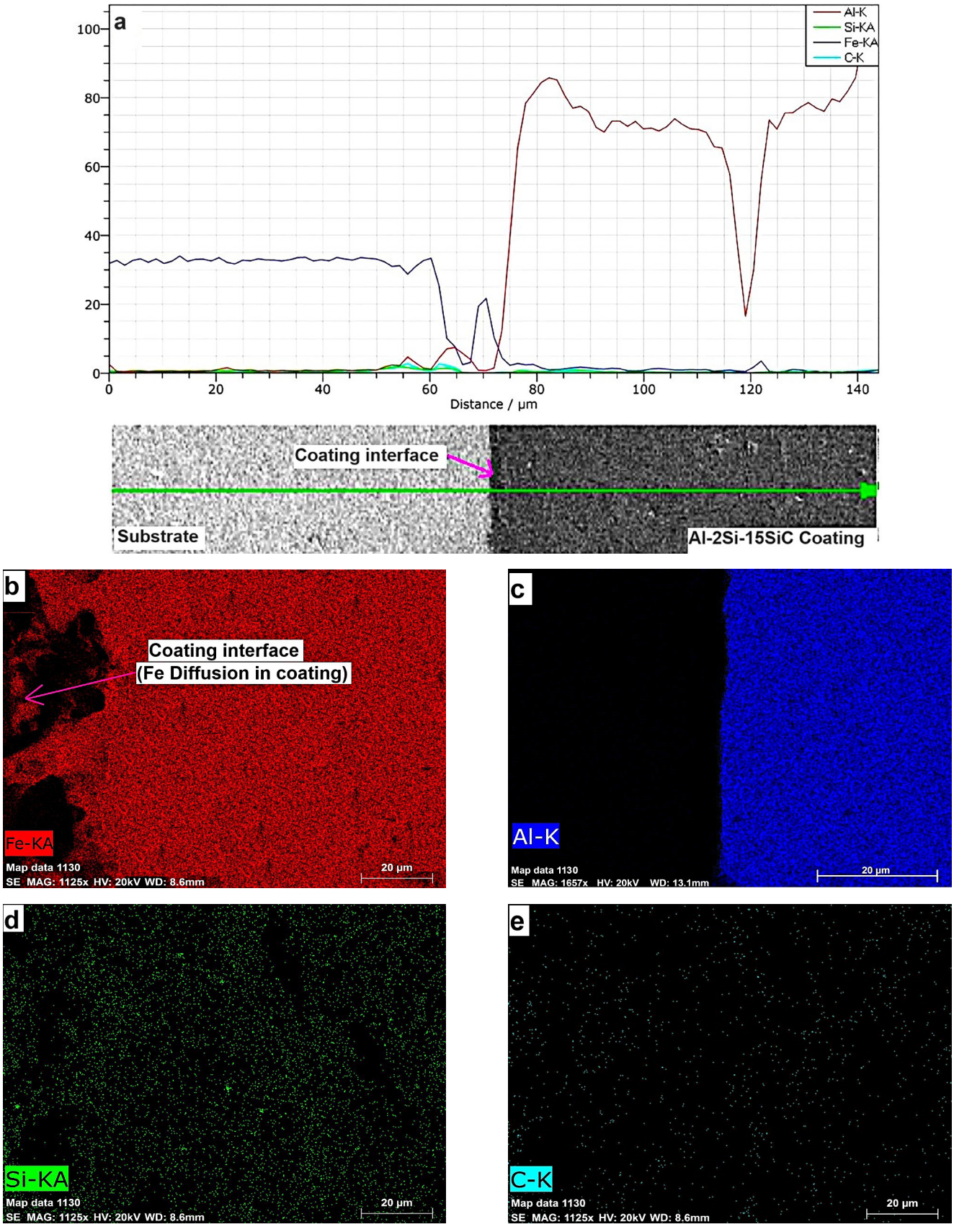

Fig. 9 EDS analysis on Al-Si-SiC: (a) Graphs of line scanning at interface from coating surface to substrate, (b) Al distribution at coating and interface region, (c) Fe distribution at coating and interface region, (d) Si distribution, (e) Carbon distribution

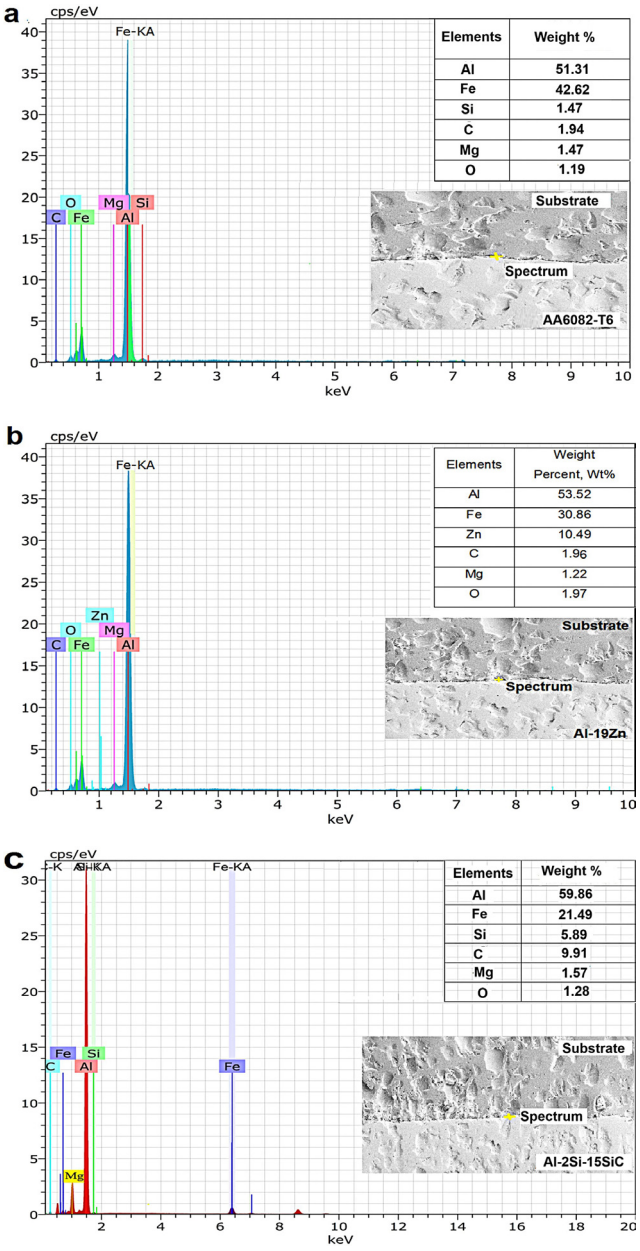

Fig. 10 (a) Elemental distribution at AA6082-T6 coating and substrate interface, (b) Elemental distribution at Al-19 coating and substrate interface, (c) Elemental distribution at Al-2Si-15SiC coating and substrate interface

3.3 Coating bond strength

The specimen loaded in the UTM is depicted in Fig. 11 (b), and using the ram tensile test, the bond strength values in MPa were determined. All twelve samples prepared (shown in Fig. 11 (a)) are put through a ram tensile test, and the results show that the FS process parameter greatly influences the coating bond strength. The bond strength values obtained for all the twelve samples tested are given in Table 4. For a lower spindle speed of 900 rpm and a lower forging pressure of 4 bar, the bond strength has decreased, while for a spindle speed of around 1100

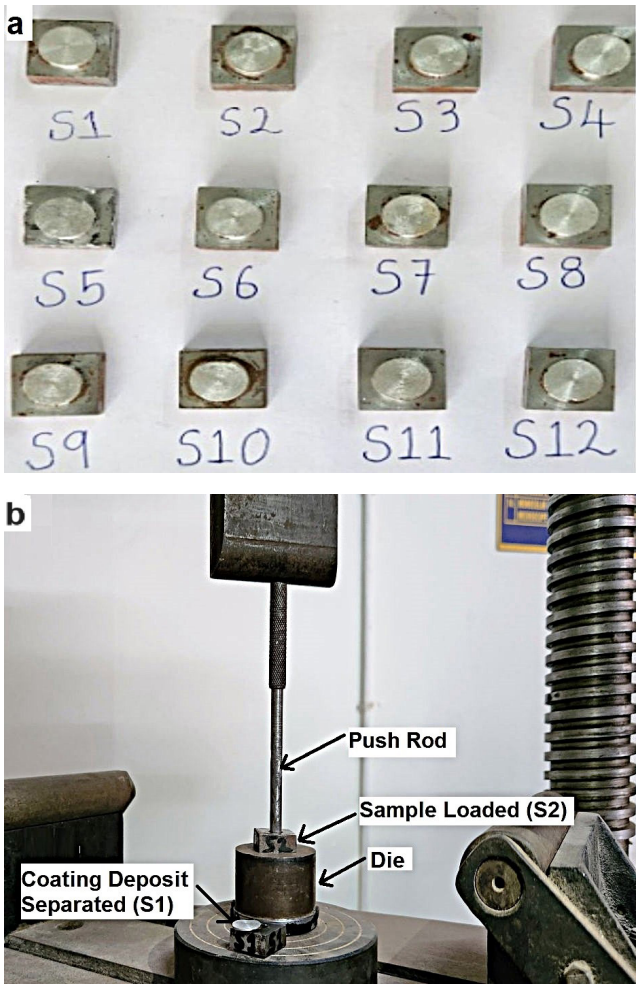

Fig. 11 (a) Sample prepared for ram tensile testing, (b) Sample loaded in UTM

to 1200 rpm and an increased forging pressure of 5 bar, the bond strength has drastically increased. Moreover, it is found that a further increase in rpm of 1400 shows poor bonding strength. The samples S3, S4, S6, S10, S11, and S12 show a good bonding strength of more than 130 MPa. Whereas the average range of coating bond strength achieved in fusion-type coating of aluminum on steel is around 20–40 MPa [44], Here, the maximum bonding strength of 142 MPa is observed in the Al-Si-SiC coating deposit for sample S10. In the case of 4 bar pressure, the samples (S1, S2, S5, and S8) tested showed a bonding strength value less than 110 MPa. It has been found that higher axial loads combined with significant rotational and traversal speeds increase the bonding strength.

3.4 Micro hardness

The hardness of the three distinct coating surfaces and the consumable rod is assessed using Vicker's microhardness test. The average hardness value observed from the coating deposit as well as from the raw consumable rod used

in FS is shown in Fig. 12. Al-2Si-15SiC coating deposits (S10 and S11) have a maximum hardness value of 148 HV. Then the hardness value of the Al-19Zn coating is found to be higher when compared with the Al6082-T6 coating deposit. This demonstrates that the coating layer's hardness has improved when compared to the consumable rod. It is clearly observed that for all three different types of Al composite coating, the hardness value of the coated surface is increased by about 15–16% in comparison with the hardness of consumable rod. A finer equiaxial grain microstructure within the coating, as opposed to the rod's anisotropic microstructure, is the cause of this improvement in the hardness of the coating surface [39]. The ultra-fine-grained microstructure produced on the coating deposit layer during FS is due to the high forging force. Because of the intense plastic deformation brought on by FS, the coated surface exhibits a sub-micrometric granular structure within the grains, which enhances the hardness [5].

3.5 Immersion tests

The coated and uncoated samples submerged in various pH media are depicted in Fig. 13. Every 24 hours, the weight reduction is calculated, and the calculated data are displayed in Fig. 14. The experiment's findings revealed that the weight loss of the three different aluminum composition-coated samples was smaller than that of the uncoated substrate material. Additionally, it is noted that for all samples assessed in various pH solutions, weight loss increases as immersion time increases. When compared to immersion in pH 3 and pH 5, the weight loss seen at pH 7 and pH 9 is significantly less, which confirms that

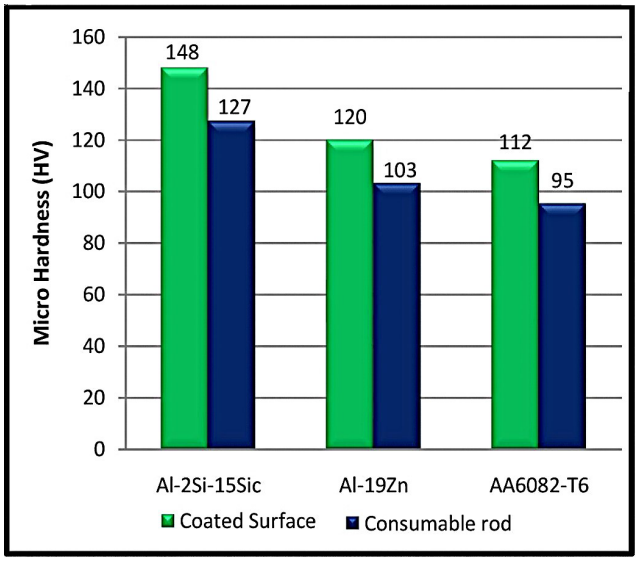

Fig. 12 Vickers micro hardness for coated surfaces and consumables used for coating

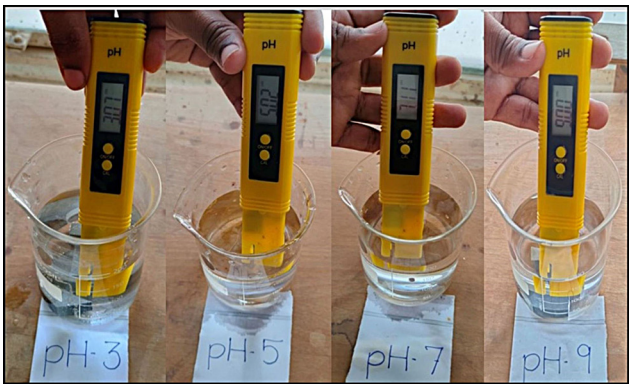

Fig. 13 Immersion corrosion test in different pH solutions

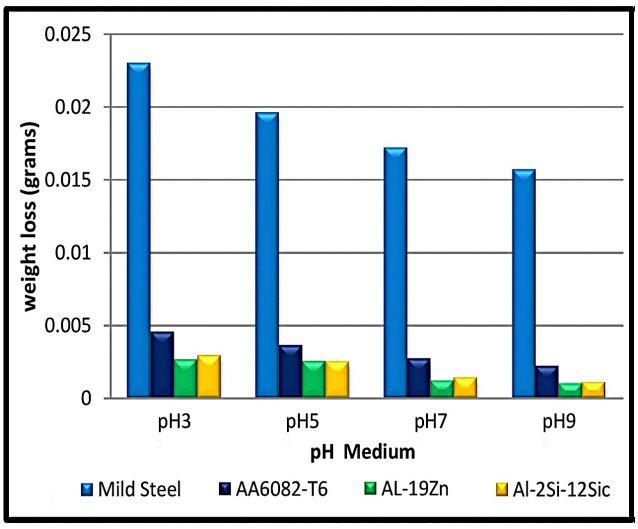

Fig. 14 Weight loss observed for 120 h of immersion in various pH media

the corrosion resistance of the coated sample is higher in the alkaline media. Equation (2) is applied to calculate the corrosion rate (CR) using the weight loss data in an alkaline environment [5, 45–47]:

$$\mathrm{CR} = \frac{K \times m}{A \times t \times \rho}, \tag{2}$$

where K – conversion constant (8.76×10^4), m – mass loss (g), A – surface area exposed (cm^2), t – immersion time (h), ρ – material density (g/cm^3) and corrosion factor (mm/year).

The corrosion rate assessed for various time periods is illustrated in Fig. 15. It is found that the corrosion rate is higher at the first 24 h of immersion, then drastically reduced due to the formation of an aluminum oxide layer in the coating deposit. The corrosion rate continues to decrease even after refilling the solution every 24 h, indicating that saturation is not the underlying cause. The production of oxide layers and their impact on corrosion resistance, with experimental evidence indicating that oxide layer formation reduces corrosion rates independent of

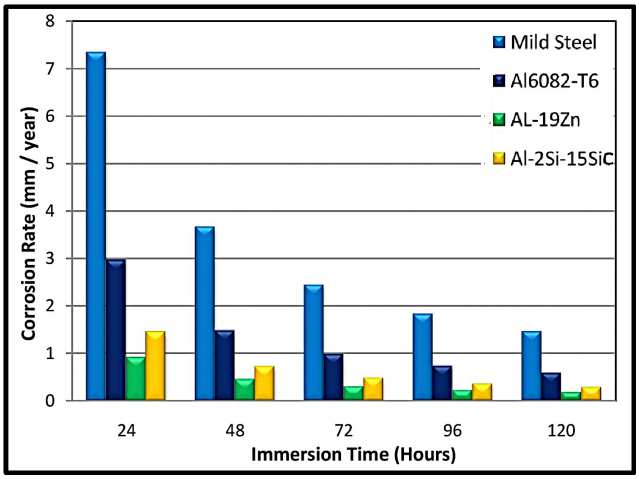

Fig. 15 Corrosion rate at various immersion times

solution saturation [48, 49]. Instead, it is supported by the development of a protective oxide layer. The corrosion rate observed for uncoated steel is higher in comparison with the other three coated samples. Then, while comparing the rate of corrosion for three different aluminum composition coating materials, it was clearly found that Al-19Zn and Al-2Si-15SiC show lower levels of corrosion rate in comparison with the AA6082-T6 coating.

3.6 Pitting corrosion test

The electrochemical polarization test curve produced by the GillAC software for the coated and uncoated samples submerged in the 3.5 weight % NaCl medium is shown in Fig. 16. Table 6 displays the corrosion current (I_{corr}) and corrosion potential (E_{corr}), which are derived from the electrochemical data obtained from potentiodynamic diagrams. The relationship between corrosion current and corrosion rate is direct [8, 9]. Uncoated steel has a higher I_{corr} of 23 µA/cm^2, while the other three coated samples' shows lower values range from 4.2 to 10.5 A/cm^2. According to the I_{corr} values, it is observed that untreated steel corrodes more quickly than the three samples that were coated with various compositions of aluminum. These results show that coated steel has significant corrosion protection provided by the coating, whereas uncoated steel is sensitive to corrosive conditions. The uncoated steel exhibits an increasing corrosion current, which leads to rapid deterioration of the material over time. The composite-coated steel does, however, exhibit some passive protection when exposed to anodic polarization [50]. The corrosion rate of the samples was calculated using the I_{corr} measurements through Faraday's law [2, 36] given by Eq. (3):

$$\mathrm{CR} = 3.27 \times \frac{I_{corr} \times \mathrm{EW}}{\rho} \tag{3}$$

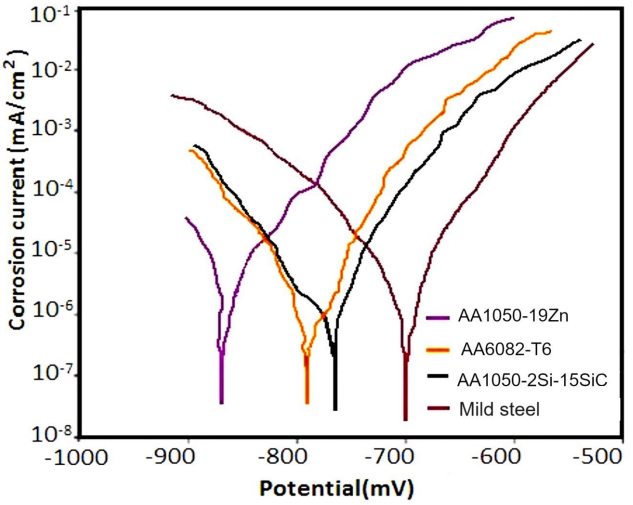

Fig. 16 Potentiodynamic diagram – 3.5 weight % NaCl immersion at 25 °C

Table 6 Electro chemical polarization test report

Sample	E_{corr} (mV)	I_{corr} (µA/cm^2)	Corrosion rate (µm/year)
Mild Steel	−718	23	272
AA6082-T6	−790	9	97
Al-19Zn	−875	10.5	78
Al-2Si-15Sic	−765	4.2	45

$$\text{Average equivalent weight} = \sum(\text{weight fraction} \times \text{equivalent weight}), \tag{4}$$

where I_{corr} – current density (µA/cm^2), EW – equivalent weight (g/equiv), and ρ – material density (g/cm^3).

From Table 6, a lower corrosion rate of 45 µm/year is observed for Al-2Si-15SiC in comparison with the other two coatings. Consequently, it is found that the Al/SiC composite coating deposit boosts steel's resistance to corrosion in corrosive environments containing 3.5 weight % sodium chloride. More SiC particles in the coating's aluminum matrix cause a decrease in corrosion current and a slower rate of corrosion, which is likely because they prevent corrosive solutions from penetrating the substrate and coating interface. The AA6082-T6 Al-19Zn coating has also shown better corrosion resistance in comparison with the uncoated steel substrate. According to these findings, coated steel receives a large amount of corrosion protection from its coating, whereas bare steel is sensitive to corrosive situations. Al serves as the outer layer in three different aluminum composition coatings, protecting against corrosion by readily generating aluminum oxide on the surface [51, 52]. This electrochemical test shows that Al-Si-SiC coating is the best option for preventing corrosion in a chloride environment, and AA6082-T6 is also preferred.

4 Conclusions

The key findings obtained from this experimental study is listed as follows:

- By using friction surfacing, AA6082-T6, Al-19Zn, and Al-2Si-15SiC consumables were effectively deposited on mild steel substrates. The interface had good bond strength and was devoid of porosity.
- The interface layer materials exhibited elements from both the steel substrate and the aluminum composite coatings, due to thermo-mechanical reactions. It was possible to identify elemental diffusion of Fe to the coating side of the interface for each of the three different coatings.
- The high plastic flow that is created while the aluminum consumable is in motion splits the coarse metal grains into fine grains, allowing the grains to disperse evenly. When coatings are deposited, extremely fine-grained microstructures are created that are much harder than consumable rods.
- According to the results of an immersion corrosion test, Al-19Zn and Al-2Si-15SiC exhibit a lower amount of weight loss than AA6082-T6 coatings. Then, for pH 7 and pH 9, the corrosion rates of the three distinct compositions of aluminum coatings are 3 to 4 times lower than for mild steel substrates.
- In the pitting corrosion test in 3.5 weight % aqueous sodium chloride medium, the Al-2Si-15SiC coating had the lowest corrosion current (I_{corr}) and rate of corrosion when compared to the other two coatings. This electrochemical test revealed that Al-Si-SiC coating is the best option for environments with chloride.

Acknowledgement

The authors sincerely acknowledge the funding that was granted by the "Department of Science and Technology, FIST" (Grant No.SR/FST/College-/2022/1300).

References

[1] Khodair, Z. T., Khadom, A. A., Jasim, H. A. "Corrosion protection of mild steel in different aqueous media via epoxy/nanomaterial coating: preparation, characterization and mathematical views", Journal of Materials Research and Technology, 8(1), pp. 424–435, 2019. https://doi.org/10.1016/j.jmrt.2018.03.003

[2] Prince Sahaya Sudherson, D., Peter Anandkumar, P., Jinu, G. R., Arun Balasubramanian, K., Vettivel, S. C. "Experimental investigation on corrosion behavior of friction surfaced mild steel with aluminum alloy 5083-Cadmium composite", Materials Research Express, 6(8), 086587, 2019. https://doi.org/10.1088/2053-1591/ab1de9

[3] Grinon-Echaniz, R., Refait, P., Jeannin, M., Sabot, R., Paul, S., Thornton, R. "Study of cathodic reactions in defects of thermal spray aluminium coatings on steel in artificial seawater", Corrosion Science, 187, 109514, 2021. https://doi.org/10.1016/j.corsci.2021.109514

[4] Yung, T.-Y., Chen, T.-C., Tsai, K.-C., Lu, W.-F., Huang, J.-Y., Liu, T.-Y. "Thermal spray coatings of Al, ZnAl and inconel 625 alloys on SS304L for anti-saline corrosion", Coatings, 9(1), 32, 2019. https://doi.org/10.3390/coatings9010032

[5] Rondinella, A., Andreatta, F., Dorbolò, L., Offoiach, R., Capurso, G., Buffa, G., Campanella, D., Fedrizzi, L. "Study of the corrosion behaviour of welded systems for marine industry applications. in technology and science for the ships of the future", In: Proceedings of NAV 2022: 20th International Conference on Ship & Maritime Research, Genova, La Spezia, Italy, 2022, pp. 78–85. ISBN 978-1-64368-296-9 https://doi.org/10.3233/PMST220011

[6] Gandra, J., Pereira, D., Miranda, R. M., Silva, R. J. C., Vilaça, P. "Deposition of AA6082-T6 over AA2024-T3 by friction surfacing - Mechanical and wear characterization", Surface and Coatings Technology, 223, pp. 32–40, 2013. https://doi.org/10.1016/j.surfcoat.2013.02.023

[7] Pradhan, S., Ghosh, S., Barman, T. K., Sahoo, P. "Tribological behavior of Al-SiC metal matrix composite under dry, aqueous and alkaline medium", Silicon, 9(6), pp. 923–931. 2017. https://doi.org/10.1007/s12633-016-9504-y

[8] Ikubanni, P., Oki, M., Adeleke, A., Adesina, O., Omoniyi, P., Akinlabi, E. "Electrochemical studies of the corrosion behavior of Al/SiC/PKSA hybrid composites in 3.5% NaCl solution", Journal of Composites Science, 6(10), 286, 2022. https://doi.org/10.3390/jcs6100286

[9] Zakaria, H. M. "Microstructural and corrosion behavior of Al/SiC metal matrix composites", Ain Shams Engineering Journal, 5(3), pp. 831–838, 2014. https://doi.org/10.1016/j.asej.2014.03.003

[10] Chandramohan, P., SivaRangar, A., Joshua Kingsly, J., Bovas Herbert Bejaxhin, A., Ramanan, N. "Investigation of corrosion and wear behavior of Al–SiC composite", Materials Today: Proceedings, 2023. https://doi.org/10.1016/j.matpr.2023.03.440

[11] Thangaraj, J., Annamalai, K., Naiju, C. D. "Investigation of wear and corrosion behavior of aluminum metal matrix composites for automotive applications", SAE International, Warrendale, PA, USA, SAE Technical Paper 2020-28-0461, 2020. https://doi.org/10.4271/2020-28-0461

[12] Kumar Murmu, S., Chattopadhayaya, S., Cep, R., Kumar, A., Kumar, A., Kumar Mahato, S., Kumar, A., Ranjan Sethy, P., Logesh, K. "Exploring tribological properties in the design and manufacturing of metal matrix composites: an investigation into the AL6061-SiC-fly ASH alloy fabricated via stir casting process", Frontiers in Materials, 11, 1415907, 2024. https://doi.org/10.3389/fmats.2024.1415907

[13] Khiabani, A., Razeghi, K., Mahdipanah, M. M., Seyedraoufi, Z., Abdolmaleki, H., Porhonar, M., Shajari, Y., Bakhtiari, H., Nosrati, R., Razavi, S. H. "Electrochemical and mechanical characteristics of Al-$_{(x)}$SiC composite fabricated by high energy compaction", Journal of the Indian Chemical Society, 99(9), 100620, 2022. https://doi.org/10.1016/j.jics.2022.100620

[14] Park, G.-D., Yang, J. H., Lee, K.-H., Kim, H.-J., Lee, S.-H., Kang, J., Yun, Y.-S., Lee, M.-H. "Ultra-high corrosion resistance of Al-Mg-Si film on steel sheet formed by PVD Mg coating and heat treatment", Corrosion Science, 192, 109829, 2021. https://doi.org/10.1016/j.corsci.2021.109829

[15] Murmu, U. K., Roy, A., Ghosh, A., Eivani, A. R., Dutta, M., Ghosh, M. "Evaluating the performance of sputter-deposited Aluminium alloy-based coatings on steel in the light of grain orientation, surface roughness, and corrosion behavior", Canadian Metallurgical Quarterly, 61(3), pp. 251–264, 2022. https://doi.org/10.1080/00084433.2022.2035635

[16] Perez, A., Billard, A., Rébéré, C., Berziou, C., Touzain, S., Creus, J. "Influence of metallurgical states on the corrosion behaviour of Al–Zn PVD coatings in saline solution", Corrosion Science, 74, pp. 240–249, 2013. https://doi.org/10.1016/j.corsci.2013.04.048

[17] Chen, W., Wang, Z., Xu, G., Song, W., Xie, Y., Zhao, L., Xia, M., Li, W. "Friction and anti-corrosion characteristics of arc sprayed Al+Zn coatings on steel structures prepared in atmospheric environment", Journal of Materials Research and Technology, 15, pp. 6562–6573, 2021. https://doi.org/10.1016/j.jmrt.2021.11.084

[18] Ritapure, P. P., Kharde, Y. R. "SiC contents and pin temperature effect on tribological properties of Al25Zn/SiC composites", International Journal of Refractory Metals and Hard Materials, 82, pp. 234–244, 2019. https://doi.org/10.1016/j.ijrmhm.2019.04.013

[19] Selvam, N. V., Sharma, A., Ramachandran, M. "Study on corrosion characteristics of aluminum alloy Al3102 in sulfate-reducing bacteria environment and investigating the use of *Azadirachta indica* leaves extract in its control", Periodica Polytechnica Chemical Engineering, 67(3), pp. 396–406, 2023. https://doi.org/10.3311/PPch.22213

[20] Khandanjou, S., Ghoranneviss, M., Saviz, S. "The detailed analysis of the spray time effects of the aluminium coating using self-generated atmospheric plasma spray system on the microstructure and corrosion behavior", Results in Physics, 7, pp. 1440–1445, 2017. https://doi.org/10.1016/j.rinp.2017.04.014

[21] Li, H., Qin, W., Galloway, A., Toumpis, A. "Friction surfacing of aluminium alloy 5083 on DH36 steel plate", Metals, 9(4), 479, 2019. https://doi.org/10.3390/met9040479

[22] Sahoo, D. K., Guna, P., Deepan, S. "Performance analysis on deposition of aluminium 6063 over en8 medium carbon steel by friction surfacing", Materials Today: Proceedings, 64, pp. 116–123, 2022. https://doi.org/10.1016/j.matpr.2022.04.020

[23] Vasanth, R., Mohan, K., Rengarajan, S., Jayaprakash, R., Kumar, R. A. "Characterization and corrosion effects of friction surfaced IS-2062 E250 CU with AA6063", Materials Research Express, 6(12), 126579, 2019. https://doi.org/10.1088/2053-1591/ab5981

[24] Bock, F. E., Kallien, Z., Huber, N., Klusemann, B. "Data-driven and physics-based modelling of process behaviour and deposit geometry for friction surfacing", Computer Methods in Applied Mechanics and Engineering, 418, 116453, 2024. https://doi.org/10.1016/j.cma.2023.116453

[25] George Sahaya Nixon, R., Mohanty, B. S., Sathish, R. "Friction surfacing of AISI 316 over mild steel: A characteriation study", Defence Technology, 14(4), pp. 306–312, 2018. https://doi.org/10.1016/j.dt.2018.03.003

[26] Agiwal, H., Yeom, H., Sridharan, K., Rudraraju, S., Pfefferkorn, F. E. "Radius of Contact During Friction Surfacing of Stainless Steel 304L: Effect of Spindle Speed and Rod Diameter", Journal of Manufacturing Science and Engineering, 146(2), 021005, 2024. https://doi.org/10.1115/1.4063653

[27] Pirhayati, P., Jamshidi Aval, H., Loureiro, A. "Characterization of microstructure, corrosion, and tribological properties of a multi-layered friction surfaced Al–Mg–Si–Ag alloy", Archives of Civil and Mechanical Engineering, 22(4), 176, 2022. https://doi.org/10.1007/s43452-022-00497-3

[28] Sahoo, D. K., Sundar Mohanty, B., Pradeep, A. M. V., David Feby John, A. "An experimental study on friction surfaced coating of aluminium 6063 over AISI 316 stainless steel substrate", Materials Today: Proceedings, 40(Supplement 1), pp. S10–S18, 2021. https://doi.org/10.1016/j.matpr.2020.03.251

[29] Reddy, G. M., Rao, K. S., Mohandas, T. "Friction surfacing: Novel technique for metal matrix composite coating on aluminium–silicon alloy", Surface Engineering, 25(1), pp. 25–30, 2009. https://doi.org/10.1179/174329408X298238

[30] Singh, A. K., Reddy, G. M., Rao, K. S. "Pitting corrosion resistance and bond strength of stainless steel overlay by friction surfacing on high strength low alloy steel", Defence Technology, 11(3), pp. 299–307, 2015. https://doi.org/10.1016/j.dt.2015.06.002

[31] Mohanasundaram, S., Vijay, S. J., Vasanth, X. A., Rai, R. S., Kantharaj, I. "Optimization of coating thickness and coating width for friction surfaced Al6061-B_4C over Al6061", Materials Today: Proceedings, 33, pp. 939–945, 2020. https://doi.org/10.1016/j.matpr.2020.06.492

[32] Naval Ship Engineering Center "MIL-J-24445A (SH) Military Specification: Joint, Bimetallic Bonded, Aluminum to Steel", Naval Ship Engineering Center (SEC 6124), Department of the Navy, Washington, DC, USA, 1977.

[33] ASTM "ASTM B311-22 Standard Test Method for Density of Powder Metallurgy (PM) Materials Containing Less Than Two Percent Porosity", ASTM International, West Conshocken, PA, USA, 2022. https://doi.org/10.1520/B0311-22

[34] ASTM "ASTM G31-21 Standard Guide for Laboratory Immersion Corrosion Testing of Metals", ASTM International, West Conshocken, PA, USA, 2021. https://doi.org/10.1520/G0031-21

[35] ASTM "ASTM G5-14(2021) Standard Reference Test Method for Making Potentiodynamic Anodic Polarization Measurements", ASTM International, West Conshocken, PA, USA, 2021. https://doi.org/10.1520/G0005-14R21

[36] Tabaghi, A., Tavakoli, H., Kami, A. "Deposition of an Al/SiC composite coating on steel by friction surfacing: Corrosion and wear properties", Mechanics of Advanced Composite Structures, 9(2), pp. 287–296, 2022.
https://doi.org/10.22075/macs.2022.26221.1383

[37] de Carvalho Filho, C. T., Brito, P. P. "Study of corrosion behavior of friction surfacing AA6351 aluminium alloy coating on AISI 1020 low carbon steel", Materials Science Forum, 1012, pp. 401–406, 2020.
https://doi.org/10.4028/www.scientific.net/MSF.1012.401

[38] Rahmati, Z., Jamshidi Aval, H., Nourouzi, S., Jamaati, R. "Effect of mechtrode rotational speed on friction surfacing of AA2024 on AA1050 substrate", CIRP Journal of Manufacturing Science and Technology, 33, pp. 209–221, 2021.
https://doi.org/10.1016/j.cirpj.2021.03.012

[39] Pirhayati, P., Jamshidi Aval, H. "An investigation on thermo-mechanical and microstructural issues in friction surfacing of Al–Cu aluminum alloys", Materials Research Express, 6(5), 056550, 2019.
https://doi.org/10.1088/2053-1591/ab0635

[40] Bararpour, S. M., Jamshidi Aval, H., Jamaati, R. "Combined experimental-numerical analysis of A356 aluminum alloy friction surfacing on AA2024 aluminum alloy substrate", Journal of Materials Research and Technology, 25, pp. 4860–4875, 2023.
https://doi.org/10.1016/j.jmrt.2023.06.265

[41] Aldawoudi, K., Varanasi, D., Baumli, P., Kaptay, G. "Wetting transition of liquid tin on the surfaces of initially oxidized steels", Transactions of the Indian Institute of Metals, 77(1), pp. 253–259, 2024.
https://doi.org/10.1007/s12666-023-03077-y

[42] Varanasi, D., Aldawoudi, K. E., Baumli, P., Koncz-Horvath, D., Kaptay, G. "Non-wetting to wetting transition temperatures of liquid tin on surfaces of different steel samples corresponding to their spontaneous deoxidation", Archives of Metallurgy and Materials, 66(2), pp. 469–476, 2021.
https://doi.org/10.24425/amm.2021.135880

[43] Sahoo, D. K., Chaudhary, S. B., Neupane, N., Babu, B. H. "Improving the mechanical and corrosion behaviour of friction surfaced aluminium deposition by forced convection nitrogen shielding technique", Journal of The Institution of Engineers (India): Series D, 105(1), pp. 503–516, 2024.
https://doi.org/10.1007/s40033-023-00496-5

[44] Kromer, R., Costil, S., Verdy, C., Gojon, S., Liao, H. "Laser surface texturing to enhance adhesion bond strength of spray coatings – Cold spraying, wire-arc spraying, and atmospheric plasma spraying", Surface and Coatings Technology, 352, pp. 642–653, 2018.
https://doi.org/10.1016/j.surfcoat.2017.05.007

[45] Malaret, F. "Exact calculation of corrosion rates by the weight-loss method", Experimental Results, 3, e13, 2022.
https://doi.org/10.1017/exp.2022.5

[46] Kutz, M. "Handbook of environmental degradation of materials", William Andrew, 2013. ISBN 978-1-4377-3455-3
https://doi.org/10.1016/C2010-0-66227-4

[47] American Chemical Society "Corrosion Handbook: Corrosive Agents and Their Interaction with Materials, Volume 7: Sodium Chloride, Competely Revised and Extended 2nd ed By G. Kreysa and M. Schütze (DECHEMA Society e.V. for Chemical Engineering and Biotechnology, Frankfurt, Germany). DECHEMA e.V.: Frankfurt and Wiley-VCH Verlag GmbH & Co. KGaA: Weinheim. 2007. xiv + 854 pp. $500. ISBN 978-3-527-31123-1.", Journal of the American Chemical Society, 129(38), p. 11874, 2007.
https://doi.org/10.1021/ja0769797

[48] Verma, C., Ebenso, E. E., Quraishi, M. A., Hussain, C. M. "Recent developments in sustainable corrosion inhibitors: design, performance and industrial scale applications", Materials Advances, 2(12), pp. 3806–3850, 2021.
https://doi.org/10.1039/D0MA00681E

[49] Ralston, K. D., Birbilis, N. "Effect of grain size on corrosion: A review", Corrosion, 66(7), pp. 075005–075005-13, 2010.
https://doi.org/10.5006/1.3462912

[50] Liu, D., Shen, M., Tang, Y., Hu, Y., Zhao, L. "Effect of multipass friction stir processing on surface corrosion resistance and wear resistance of ZK60 alloy", Metals and Materials International, 25(5), pp. 1182–1190, 2019.
https://doi.org/10.1007/s12540-019-00268-5

[51] Gnanasekaran, M., Mohan, K., Kumaravel, A., Magibalan, S. "Characterization, corrosion behavior, effect of temperature and inhibition studies on AA6351 frictional surfaced mild steel", Journal of Materials Research and Technology, 9(6), pp. 16080–16092, 2020.
https://doi.org/10.1016/j.jmrt.2020.11.065

[52] Farajollahi, R., Jamshidi Aval, H., Jamaati, R., Javidani, M. "Non-isothermal aging behavior of a friction-surfaced Al-Cu-Mg alloy matrix composite coating reinforced by nickel-aluminide", Journal of Central South University, 30(11), pp. 3696–3708, 2023.
https://doi.org/10.1007/s11771-023-5438-x